



Redox stable Ni–YSZ anode support in solid oxide fuel cell stack configuration

Antonin Faes^{a,b,*}, Zacharie Wuillemin^c, Pietro Tanasini^{b,d}, Nicola Accardo^a, Jan Van Herle^b

^a Interdisciplinary Centre for Electron Microscopy (CIME), Ecole Polytechnique Fédérale de Lausanne (EPFL), CH-1015 Lausanne, Switzerland

^b Industrial Energy Systems Laboratory (LENI), EPFL, CH-1015 Lausanne, Switzerland

^c HTceramix – SOFCpower, 26 Avenue des Sports, CH-1400 Yverdon-les-Bains, Switzerland

^d Group of Electrochemical Engineering (GGEC), EPFL, CH-1015 Lausanne, Switzerland

ARTICLE INFO

Article history:

Received 30 August 2010

Received in revised form 17 October 2010

Accepted 7 November 2010

Available online 18 November 2010

Keywords:

SOFC

Redox cycles

Reduction and oxidation cycles

Nickel and yttria-stabilized zirconia

Anode-supported cells

Electrochemical impedance spectroscopy

ABSTRACT

State-of-the-art nickel-based SOFC anode-supported cells are highly sensitive to reoxidation of the metal phase at the temperature of utilization. This work presents results on redox stable nickel–YSZ (yttria-stabilized zirconia) anode-supported cells, for both smaller and larger scale cells. A 55 cm² cell was mounted in a SOFC stack repeat element and tested over 40 full redox cycles. Performances and electrochemical impedance results of the repeat element are compared to the smaller sized cells of similar anode support structure.

© 2010 Elsevier B.V. All rights reserved.

1. Introduction

Solid oxide fuel cell devices (SOFC) are promising energy conversion means due to high electrical efficiency even for small power systems [1]. The nickel–YSZ (yttria-stabilized zirconia) anode-supported cell configuration has established itself as a standard, due to reduced ohmic losses and reasonably low degradation. Its major limitation, however, is the low mechanical stability when changing from reducing to oxidizing atmosphere [2]. Nickel re-oxidation at high temperature creates a porous oxide structure, which induces an expansion of the anode support that may crack the thin electrolyte layer [3]. Larger scaled systems can include an external safety gas protection procedure to prevent re-oxidation of the anode in case of lack of fuel [4]. To remain competitive, small-scale systems should work without such purge gas and need redox stable anode-supported cells. Only a few works so far presented Ni–YSZ anode-supported cells of fair size (area >50 cm²) that can withstand full redox cycles without total loss of OCV (open circuit voltage) [4–6].

This paper reports the upscaling of a previous anode-supported cell microstructure tested under redox cycling of small cells [7].

That anode microstructure had been optimized using a design of experiment approach [8].

2. Experimental

Half-cells were produced by water-based tape-casting using ammonium polyacrylate dispersant and polyacrylic binder (see Ref. [7] for further details). The electrolyte was composed of 8 mol% yttria (Y₂O₃) stabilized zirconia (ZrO₂) (8YSZ). Two anode support ceramic compositions were tested: (1) 40 wt% NiO, 60 wt% 8YSZ (named as T40) and (2) 40 wt% NiO, 59 wt% 8YSZ, 1 wt% Al₂O₃ (named as T40a). The alumina was added as a sintering aid and to increase the anode support strength [9]. To increase the as-sintered porosity, 3 wt% of rice starch pore-former was added. Co-sintering of anode and electrolyte was done at 1400 °C for 4 h in air (Nabertherm HT10/18, Germany). After firing, the anode substrate and thin electrolyte thicknesses amount to around 600 and 15 μm, respectively. The cathode was composed of 50:50 vol% of LSM ((La_{0.75}Sr_{0.25})_{0.95}MnO_{3-d}, Praxair, Inc., USA) and 8YSZ (Tosoh Corp., Japan). An anode current collecting layer based on 90 wt% NiO (J.T. Baker, Inc., USA) and 10 wt% 8YSZ (Tosoh Corp., Japan) and a cathode current collecting layer of La_{0.5}Sr_{0.5}CoO_{3-x} (Praxair, Inc., USA) were deposited by brush on the respective electrodes. Two cell dimensions were tested for the anode support containing alumina, a small and a large cell with sizes of 14.5 and 55 cm², respectively. Only a small cell was tested for the anode support without alumina. The cathode

* Corresponding author at: Industrial Energy Systems Laboratory (LENI), Ecole Polytechnique Fédérale de Lausanne (EPFL), Station 9, CH-1015 Lausanne, Switzerland. Tel.: +41 21 693 6813; fax: +41 21 693 3502.

E-mail address: antonin.faes@a3.epfl.ch (A. Faes).

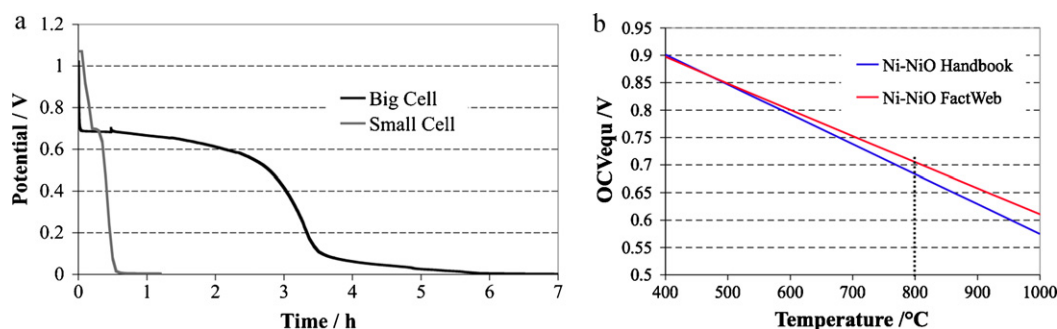


Fig. 1. Open circuit voltage (OCV) (a) versus time of oxidation for the two cell configurations and (b) versus temperature for the Ni/NiO equilibrium [13,14].

areas were 1 and 48 cm² for the small and large cells, respectively.

The smaller cell was tested as described in Ref. [7] with 300 ml min⁻¹ humidified (around 3% H₂O) H₂ and 450 ml min⁻¹ air. The contact meshes were platinum for the cathode and nickel for the anode. Electrochemical impedance spectroscopy (EIS) measurements (frequency sweep between 1 MHz and 1 Hz) and current–voltage curves (sweep scan of 3 mV s⁻¹) were performed with an Eco Chemie Autolab®. Only the small cell T40a was tested by EIS.

The larger cell was tested in SOFC stack repeat element configuration in a so-called “S-design” setup [10] including metallic bipolar plates and proprietary gas diffusion and contacting layers. The total fluxes were 10 ml min⁻¹ cm⁻² of humidified 50% dilute H₂ in N₂ for the anode side and 120 ml min⁻¹ cm⁻² of air for the anode side. The mechanical load was 1 kg cm⁻². EIS measurements (frequency sweep between 100 kHz and 0.1 Hz) were performed with a Zahner Elektrik IM6 instrument, with an external PP240 potentiostat for *i*-*V* recording.

Full redox cycles were applied by first purging for 5 min the fuel side with nitrogen for safety reasons and then letting the nickel reoxidize by air leakage through the sealing for the large cell and by flowing air over the anode for the small cells. All the redox cycles were carried out at 800 °C except for the 12th redox cycle of the small cell T40, which was done at 850 °C. Fig. 1a plots the potential evolution of the cells during reoxidation time at 800 °C. The minimal time of oxidation was fixed to 1½ h for the small cells and 6 h for the repeat element configuration; in some cases the oxidations were done during the night or a full weekend, without noticing any influence on the results.

Microstructure observations were done using a scanning electron microscope (Zeiss NVision 40 Crossbeam) equipped with a Schottky field emission gun, a Gemini column and an energy selec-

tive backscattered electron detector (EsBSE). The samples were impregnated with epoxy embedding kit (Fluka No. 45359) and polished using diamond lapping films down to 1 μm with water as lubricant and cooling medium [7].

To compare microstructures after aging, the as-sintered and tested cells (after electrochemical redox cycling test) were soaked in a tubular furnace (Lenton, UK) at 800 °C during 300 h under humidified diluted hydrogen (10% H₂ in nitrogen).

3. Results and discussion

The kinetics of oxidation are different for the two different cell sizes. This is first due to the different total Ni amount to be oxidized and second to the different test geometries. The smaller cell is in an open configuration (uncontrolled post-combustion around the cell) that lets the air (and produced steam) back-diffuse into the anode compartment. In comparison, the larger cell setup is sealed and the fuel gases are extracted from the furnace in a condenser without post combustion. Back diffusion of air can occur through the fuel gas exit, the sealing and silicone tubing of the fuel inlet. Both cells show a plateau around 0.7 V during nickel reoxidation. The open circuit voltage (OCV) can be calculated using the Nernst equation and expressing the oxygen partial pressure at the anode side as a function of the standard Gibbs free energy of formation of NiO versus temperature ($\Delta G_{\text{Ni-NiO}}^{\circ}(T)$) [11,12]:

$$\text{OCV} = \frac{RT}{4F} \ln \left(\frac{p_{\text{O}_2}^{\text{cathode}}}{p_{\text{O}_2}^{\text{anode}}} \right) \quad (1)$$

with

$$p_{\text{O}_2}^{\text{anode}} = \exp \left(\frac{2\Delta G_{\text{Ni-NiO}}^{\circ}(T)}{RT} \right) \quad (2)$$

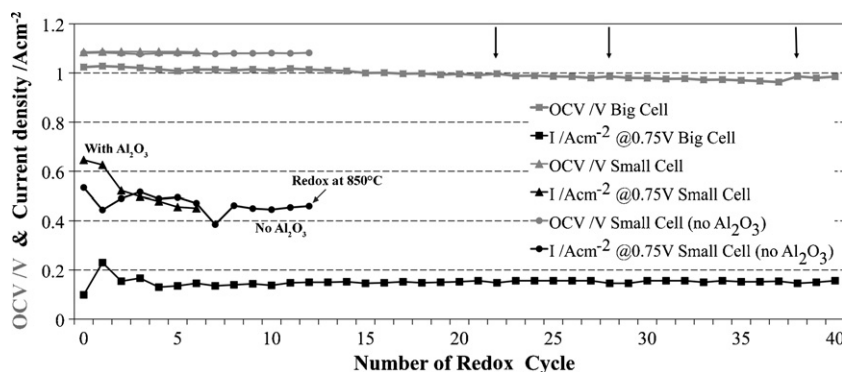


Fig. 2. Open circuit voltages (OCV) and current densities at 0.75 V for the large cell (repeat element: 48 cm² active cathode area) and small cells (1 cm² active cathode area) at 800 °C versus the number of redox cycles. The large cell and one of the small cells are composed of anode supports with 1 wt% Al₂O₃ (T40a). The other small cell does not contain alumina (T40). All redox cycles are performed at 800 °C except for the last cycle of cell T40 (850 °C). The arrows show a small OCV increase and concurrent performance decrease, after periods of cell polarization.

$$\text{OCV} = \frac{1}{2F} \left(\frac{R \ln \left(\frac{p_{\text{O}_2}^{\text{cathode}}}{p_{\text{O}_2}^{\text{anode}}} \right)}{2} T - \Delta G_{\text{Ni-NiO}}^{\circ}(T) \right) \quad (3)$$

where T is the temperature in K, R is the gas constant, F is the Faraday constant, $p_{\text{O}_2}^{\text{cathode}}$ and $p_{\text{O}_2}^{\text{anode}}$ are the partial pressures of oxygen at the cathode and the anode side, respectively. The value of OCV is given versus temperature in Fig. 1b: at 800 °C, the OCV is between 0.68 and 0.71 V depending on the value of the Gibbs free energy [13,14]. From Fig. 1b and from a practical point of view, it is interesting to note that the potential of Ni/NiO equilibrium is increased to 0.8 V if the temperature is decreased to 600 °C. This implies that the support can be more easily oxidized at this temperature under high fuel utilization, restricting the operating window of low temperature Ni-anode based SOFC.

The behavior of the three cells is given in Fig. 2. The OCV of both small cells is constant over the redox cycles. The OCV value for the small anode containing alumina is 1.087 V, which is relatively close to the theoretical Nernst potential with 3% H₂O in H₂ versus air (1.102 V at 800 °C). The larger cell shows a lower OCV value of 1.025 V under humidified 50% H₂ in N₂ (theoretical value = 1.069 V); the larger difference could be due to the lower hydrogen flux in the stack repeat element configuration: 300 versus 10 ml min⁻¹ cm⁻² for the smaller and larger cell, respectively. If the thin electrolyte contains small pinholes, the higher flux will remove steam formed at these locations.

For the larger cell, the OCV decreases by about 0.1% per redox cycle over a total of 40 cycles. Forty redox cycles is twice the required number estimated for a stack lifetime of 40,000 h [15]. The arrows in Fig. 2 show a small increase in OCV after redox cycles following a polarization period of the cell. The cell was polarized for 20, 50 and 90 h after redox cycles 21, 28 and 37, respectively. This increase in OCV after polarization could be due to healing of small cracks in the thin electrolyte, observed previously in case of anode-supported cells under reducing atmosphere [3].

The performance of the small cells (0.76 A cm⁻² at 0.6 V after 6 redox cycles for T40a and 0.78 A cm⁻² at 0.6 V after 12 redox cycles for T40) is comparable to other reported performances after multiple redox cycles for similar anode compositions [7]. In Fig. 2, the current density is given at a safe potential of 0.75 V. The small cell containing alumina (T40a) shows a decrease in performance during the first 5 redox cycles from 0.65 to 0.45 A cm⁻². The small cell without alumina (T40) starts at a lower performance (0.53 A cm⁻²) but stabilizes after 8 redox cycles at a similar current density than the small cell T40a. The larger cell presents an initial performance increase followed by a decrease to 0.13 A cm⁻² after 4 redox cycles. From this value, though, the performance increases slightly towards a stable value around 0.15 A cm⁻² within the next 8 redox cycles and then maintains this performance until the end of the test. The initial performance lowering is due to nickel coarsening during the first reduction as shown in Fig. 3a and described in a previous study [7].

Redox cycles strongly affect the nickel phase microstructure (see Fig. 3). After 300 h of reduction (under humidified dilute hydrogen), the Ni phase (grey) of T40 is dense and agglomerated (see Fig. 3a). To observe the effect of the redox cycles, the small cell T40 tested in Fig. 2 is reduced during 300 h (see Fig. 3b and c). After redox treatments, the Ni phase is porous and contains zirconia inclusions (light grey). Ni internal porosity is created during Ni oxidation due to Ni²⁺ outwards diffusion [7,16] and seems to be maintained during reduction. Longer-term reduction does not lead to a major coarsening of Ni after redox cycling probably due to the small zirconia inclusions inside the Ni grains.

To understand the important difference in performance between the cells (see Fig. 4a), electrochemical impedance spectroscopy was performed on the small and large cell anode-

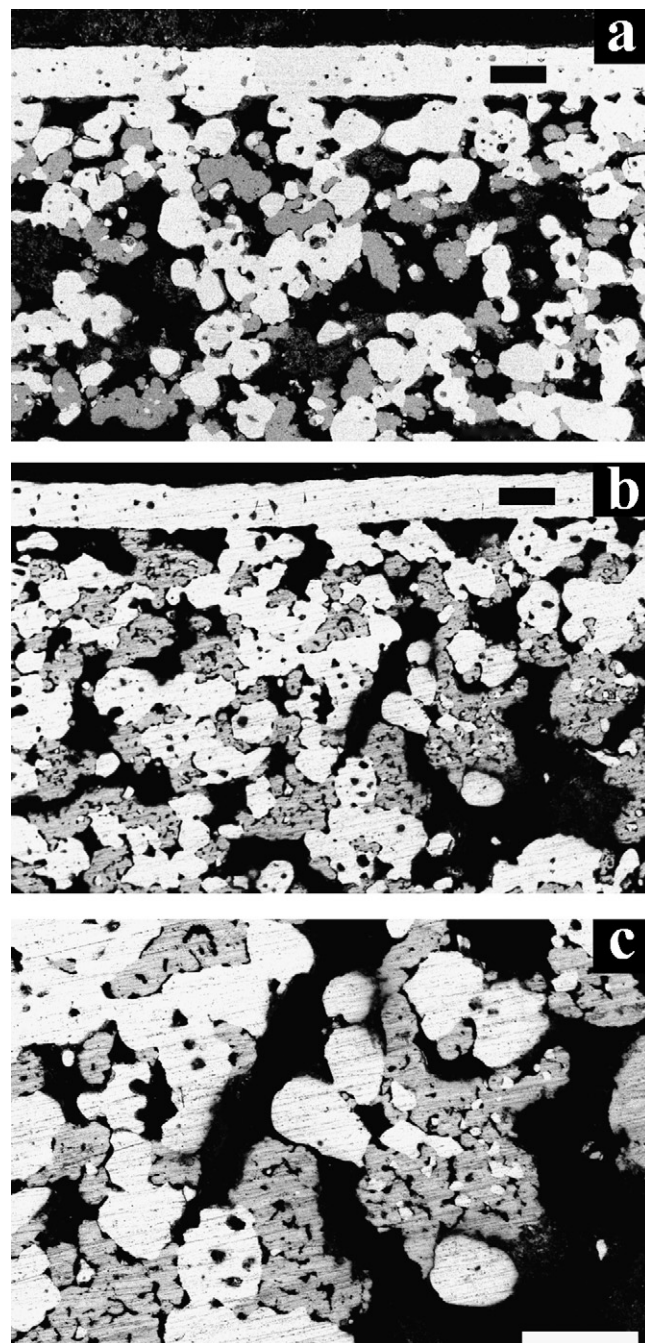


Fig. 3. Anode support (T40: 40 wt% NiO and 60 wt% YSZ) microstructure (a) after 300 h under humidified dilute hydrogen (10% H₂ in N₂), (b) and (c) after 12 redox cycles (see Fig. 2) and 300 h under humidified dilute hydrogen. Light grey (8YSZ), dark grey (Ni) and black (pores). Data bar length is always 10 µm. Conditions: ESBSSE detector, 1.9 kV.

supported cells containing alumina (T40a) (see Fig. 4b). A first major difference is apparent from the ohmic resistances (series resistance R_s , high frequency intercept), which include electrode contacting, ohmic loss in the electrodes and in the electrolyte. For the larger cell, this R_s is almost double the one of the small cell (see Table 1). As the electrolyte and anode are from the same batches, and the cathode from the same composition, no intrinsic cell difference should exist. The major difference in R_s may probably stem from a contacting issue of the electrodes in the large cell stack configuration.

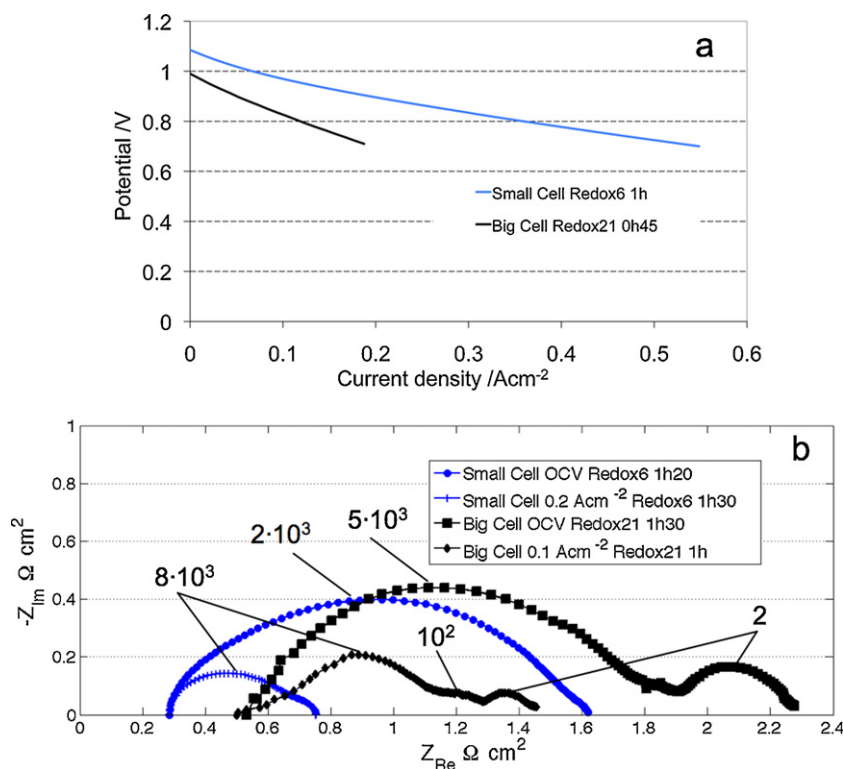


Fig. 4. (a) Current–voltage curves for the small and large cells (both with anode containing 1 wt% Al₂O₃, T40a). (b) Nyquist plot of small cell versus large cell at open circuit voltage (OCV) and under polarization (0.2 and 0.1 A cm⁻² for small and large cell, respectively). *Small cell conditions:* 300 ml min⁻¹ cm⁻² humidified H₂, 450 ml min⁻¹ cm⁻² air at 800 °C. *Large cell conditions:* 10 ml min⁻¹ cm⁻² humidified 50% H₂ in N₂, 120 ml min⁻¹ cm⁻² air at 800 °C. The ac impedance signal frequencies of relevant measurement points are indicated in the graph and discussed in the text.

A second difference lies in the polarization resistance responses (R_p), which represent the electrochemical losses, including among others gas conversion, gas diffusion and charge transfer loss at the electrodes. The large cell shows a polarization resistance about double that the one of the small cell, under dc current bias; at OCV condition, however, the R_p difference is only ca. 30%. The reasons for the higher R_p for the larger cell were analyzed to originate from: (a) the response around 2 Hz not present in the small cell and that can be attributed to the anode gas conversion impedance due to the lower flux and the dilution of hydrogen in nitrogen [17]. The gas conversion impedance arc is due to the change in composition in the channel above the cell during low frequency impedance measurement itself; the second reason of R_p increase is (b) a small additional response peak observed around 100 Hz under polarization, which could be attributed to the anode gas diffusion process [18]. The high frequency peak between 2 and 8 kHz is related to charge transfer at the Ni–YSZ anode [19]. The resistance of this response arc raises with increasing particle size [19–21], it varies

Table 1

Comparison of ohmic resistances (R_s), polarization resistances (R_p) and peak height of the imaginary part of impedance (Z'') for small cell (after Redox6) and large cell (after Redox21). Values correspond to Fig. 4.

Ω (cm ²)	OCV		Polarized	
	Small cell	Large cell	Small cell	Large cell
R_s	0.28	0.53	0.28	0.52
R_p	1.34	1.74	0.47	0.93
$-Z''$ (high frequency)	0.4	0.44	0.14	0.21
$-Z''$ (2 Hz)		0.17		0.07
$-Z''$ (100 Hz)				0.07

between 1 and 10 kHz for finer microstructures but can be as high as 14 kHz at 1000 °C for coarser microstructures [20,22]. In Fig. 4 and Table 1, the height of this peak is only ca. 10% higher at OCV for the large cell compared to the small cell. This difference is more pronounced under polarization (ca. 50% higher for the larger cell) but this can come from the different polarizing current (0.2 and 0.1 A cm⁻²). Since the charge transfer response is similar for both cells, the main difference in performance is thus coming from the ohmic contact, the gas conversion and diffusion limitations in the larger cell (due to test configuration, i.e. lower, dilute, fuel supply with the repeat element). Finally, the open circuit voltage is also lower for the large cell.

Degradation of the small cell is important during the first 5 redox cycles and then stabilizes (see Fig. 2). Anode degradation is inherently present during utilization due to nickel phase coarsening which decreases the triple phase boundary (TPB) and the electrical conductivity [7,23]. Degradation of the small cell in Fig. 5 and the large cell in Fig. 6 illustrates both these effects: the increase in R_s due to the decrease of electrical conductivity, and an increase in R_p (high frequency arc) due to the decrease in electrochemical activity as a consequence of decreased TPB.

It is worth noting that the fuel utilization of the repeat element was between 14% and 32% after the first reduction and the first redox cycle, respectively. This was first due to the high area specific resistance in the large cell configuration, due to elevated contact and polarization resistance (see Figs. 4 and 6). Second, the employed test setup was dedicated for larger stack configuration with the lower limit of the H₂ flow fixed at 150 ml min⁻¹ (representing 3.125 ml min⁻¹ cm⁻²). For these reasons, the cell could not be tested under higher fuel utilization and gas limitation.

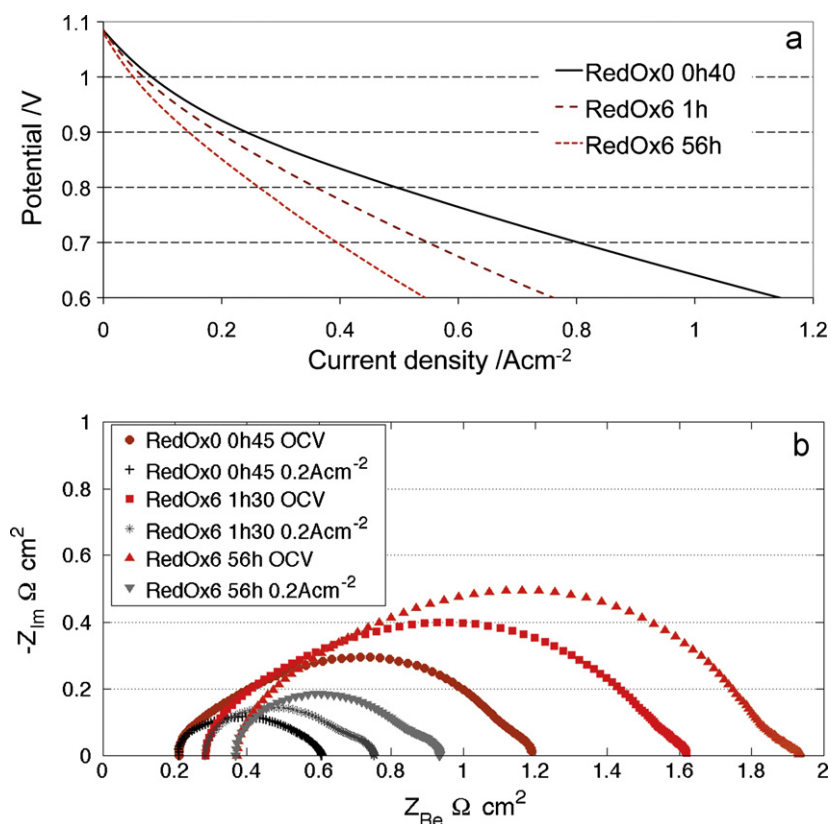


Fig. 5. Degradation of small cell T40a with redox cycles and time (a) current–voltage curve and (b) Nyquist plot. *Conditions:* 800 °C, H₂ at 300 ml min⁻¹ cm⁻² humidified with water (about 3%).

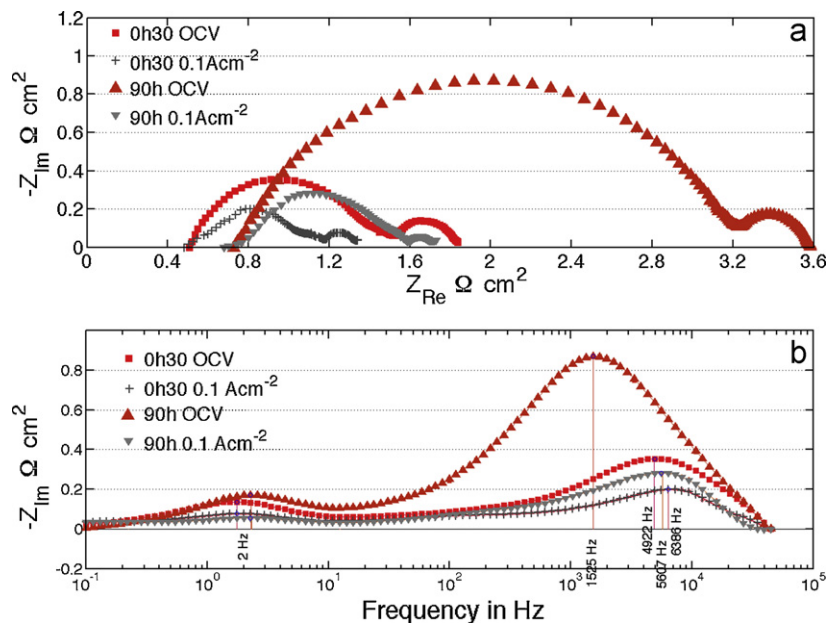


Fig. 6. Degradation of the large cell (48 cm²) with time after 37 redox cycles (a) Nyquist plot and (b) frequency peak of the imaginary part of impedance (Z_{im}). *Conditions:* 50% H₂, 10 ml min⁻¹ cm⁻², balance N₂ (humidified with water, about 3%), 800 °C.

4. Conclusion

This work presented an anode-supported cell with an active (cathode) area of 48 cm² mounted in a SOFC stack repeat element configuration that withstood 40 redox cycles with a decrease in open circuit voltage of ca. 1 mV per cycle and a stabilized output power performance after a certain number of cycles.

The oxidation time depended on the cell configuration, over 6 h for the sealed repeat element versus less than 1 h for the sealless test configuration of the small cell.

The lower performance of the repeat element compared to the small cells was related to ohmic losses from contacting and to the anode gas conversion and diffusion resistances as a consequence of reduced fuel feeding (concentration and flux) in the repeat element.

Next steps will be focused on increasing the durability and the performance of the anode by adding an anode functional layer.

Acknowledgments

Kind acknowledgements are extended to the Ceramic Laboratory (LC–EPFL, Prof. N. Setter and J. Castano) for the furnace and cell fabrication facilities and to the European Institute for Energy Research (ElFER, Karlsruhe, Germany) for the financial support (Contract No. N43/C06/019), as well as to the European Commission for funding of the FP7 project RobAnode (Grant Agreement 245355).

References

- [1] S.C. Singhal, K. Kendall, *High Temperature Solid Oxide Fuel Cell—Fundamentals-Design and Applications*, Elsevier, Oxford, 2003.
- [2] M. Cassidy, G. Lindsay, K. Kendall, *J. Power Sources* 61 (1996) 189–192.
- [3] A. Faes, A. Nakajo, A. Hessler-Wyser, D. Dubois, S. Modena, A. Brisse, J. Van Herle, *J. Power Sources* 193 (2009) 55–64.
- [4] A. Wood, M. Pastula, D. Waldbillig, D. Ivey, S.C. Singhal, J. Mizusaki (Eds.), *SOFIX—Electrochemical Society Proceedings Volume 2005–2007*, Quebec, Canada, 2005, pp. 571–583.
- [5] G. Robert, A. Kaiser, E. Batawi, M. Mogensen (Eds.), *Sixth European Solid Oxide Fuel Cell Forum*, Lucerne, Switzerland, 2004, p. 193.
- [6] R. Ihringer, *European Fuel Cell Technology and Applications—Pietro Lunghi Conference*, Rome, Italy, 2009, pp. 187–188.
- [7] A. Faes, Z. Wuillemin, P. Tanasini, N. Accardo, M. Cantoni, H.J. Schindler, H. Luebbe, S. Diethelm, A. Hessler-Wyser, J. Van Herle, *J. Power Sources*, doi:10.1016/j.jpowsour.2010.11.146.
- [8] A. Faes, J.M. Fuerbringer, D. Mohamedi, A. Hessler-Wyser, G. Caboche, J. Van Herle, *J. Power Sources*, doi:10.1016/j.jpowsour.2010.07.092.
- [9] T. Klemensoe, C. Chung, P.H. Larsen, M. Mogensen, *J. Electrochem. Soc.* 152 (2005) 2186–2192.
- [10] O. Bucheli, M. Molinelli, T. Zahringer, E. Thorn, S. Diethelm, Z. Wuillemin, A. Nakajo, N. Autissier, J. Van Herle, *ECS Trans.* 7 (2007) 123–132.
- [11] J. Van Herle, D. Larrain, N. Autissier, Z. Wuillemin, M. Molinelli, D. Favrat, *J. Eur. Ceram. Soc.* 25 (2005) 2627–2632.
- [12] D. Sarantaridis, R.A. Rudkin, A. Atkinson, *J. Power Sources* 180 (2008) 704–710.
- [13] G.D. Handbook, Elsevier, 2010, http://xfire.mimas.ac.uk/crossfire/ov_gmelin.html.
- [14] C.W. Bale, 2007, <http://www.crct.polymtl.ca/factweb.php>.
- [15] A. Mai, B. Iwanschitz, R. Denzler, D. Haberstock, A. Schuler, P. Connor (Eds.), *Ninth European Solid Oxide Fuel Cell Forum*, Lucerne, Switzerland, 2010, pp. 2–144.
- [16] D. Sarantaridis, R.J. Chater, A. Atkinson, *J. Electrochem. Soc.* 155 (2008) B467–B472.
- [17] S. Primdahl, M. Mogensen, *J. Electrochem. Soc.* 145 (1998) 2431–2438.
- [18] S. Primdahl, M. Mogensen, *J. Electrochem. Soc.* 146 (1999) 2827–2833.
- [19] S. Primdahl, M. Mogensen, *J. Electrochem. Soc.* 144 (1997) 3409–3419.
- [20] C.H. Lee, H.Y. Lee, S.M. Oh, *Solid State Ionics* 98 (1997) 39–48.
- [21] B. Iwanschitz, A. Mai, L. Holzer, T. Hocker, M. Schütze, P. Connor (Eds.), *Ninth European Solid Oxide Fuel Cell Forum*, Lucerne, Switzerland, 2010, pp. 7–61.
- [22] S. Primdahl, *Nickel/Yttria-Stabilised Zirconia Cermet Anodes for Solid Oxide Fuel Cells*, Risoe National Laboratory, DTU, Roskilde, 1999.
- [23] A. Faes, A. Hessler-Wyser, D. Presvytes, C.G. Vayenas, J. Van Herle, *Fuel Cells* 9 (2009) 841–851.